APPENDIX A: SELF-GRAVITATION

Let us consider $\mathtt{U}(r)$, $\mathtt{V}(r)$ and $\mathtt{P}(r)$ the eigenfunctions describing the radial and transverse displacement and the gravitational potential. The exact solutions for spheroidal oscillations of a uniform Earth are developed e.g. in Pekeris & Jarosch (1958) and Takeuchi & Saito (1972). The eigenfrequencies and eigenfunctions of a uniform Earth computed in the present study, both in non self-gravitating and self-gravitating models, are based on their results. We use the Mineos package (Woodhouse 1988) to compute the free oscillations of the PREM model. The Mineos package does not routinely compute and output $\mathtt{P}(r)$ eigenfunctions when self-gravitation is shut down. Hence, a subroutine performing the following integration (Pekeris & Jarosch 1958) was added to the Mineos package:

$$\mathtt{P}(r) \;=\; -\,\frac{4\pi G}{2\ell+1}\left[\,\frac{1}{r^{\,\ell+1}}\int_0^r \rho_0(r')\left[\,\ell\,\mathtt{U}(r') \;+\; k\,\mathtt{V}(r')\,\right] r'^{\,\ell+1}\,dr' \right.$$
$$\left. +\; r^{\,\ell}\int_r^a \rho_0(r')\left[\,-\,(\ell+1)\,\mathtt{U}(r') \;+\; k\,\mathtt{V}(r')\,\right]\frac{1}{r'^{\,\ell}}\,dr'\,\right]. \qquad \text{(A.1)}$$

It can be noted that this expression is the normal mode equivalent formulation of equation (4).

Fig. A1 displays the dispersion diagram of non self-gravitating and self-gravitating PREM models. The effect of self-gravitation on eigenfrequencies is noticeable up to a few mHz and $\ell < 10$. A similar effect is seen in Fig. A2 for the fundamental eigenfunctions $\dot{\mathtt{P}}(r)$ of a homogeneous solid sphere. The vertical gravity perturbations g_1 induced by the Tohoku-oki earthquake at INU and MDJ stations are displayed in Fig. A3, both in non self-gravitating and self-gravitating PREM models. The long-period trend differs slightly between the two Earth models.

APPENDIX B: HORIZONTAL COMPONENTS

The horizontal gravity perturbations g_1 at P-wave arrival time induced by the M9.1 Tohoku-oki rupture are displayed in Figs A4 (north component) and A5 (east component), in the self-gravitating PREM model. Radiation patterns differ significantly from the vertical radiation pattern presented in Fig. 8. However, the amplitudes of the horizontal perturbations at P-wave arrival time also exceed $1\mathrm{nm/s}^2$, meaning that their detection is today prevented by the noisier character of the horizonal components of the broadband seismometers, but not by their weaker amplitude.

REFERENCES

Pekeris, C. L. & Jarosch, H., 1958. The free oscillations of the Earth, in *Contributions in Geophysics in Honor of Beno Gutenberg*, pp. 171–192, Pergamon Press.

Takeuchi, H. & Saito, M., 1972. Seismic surface waves, in *Methods in Computational Physics: Advances in Research and Applications*, pp. 217–295, Elsevier.

Woodhouse, J. H., 1988. The calculation of the eigenfrequencies and eigenfunctions of the free oscillations of the Earth and the Sun, in *Seismological Algorithms: Computational Methods and Computer Programs*, Academic Press.

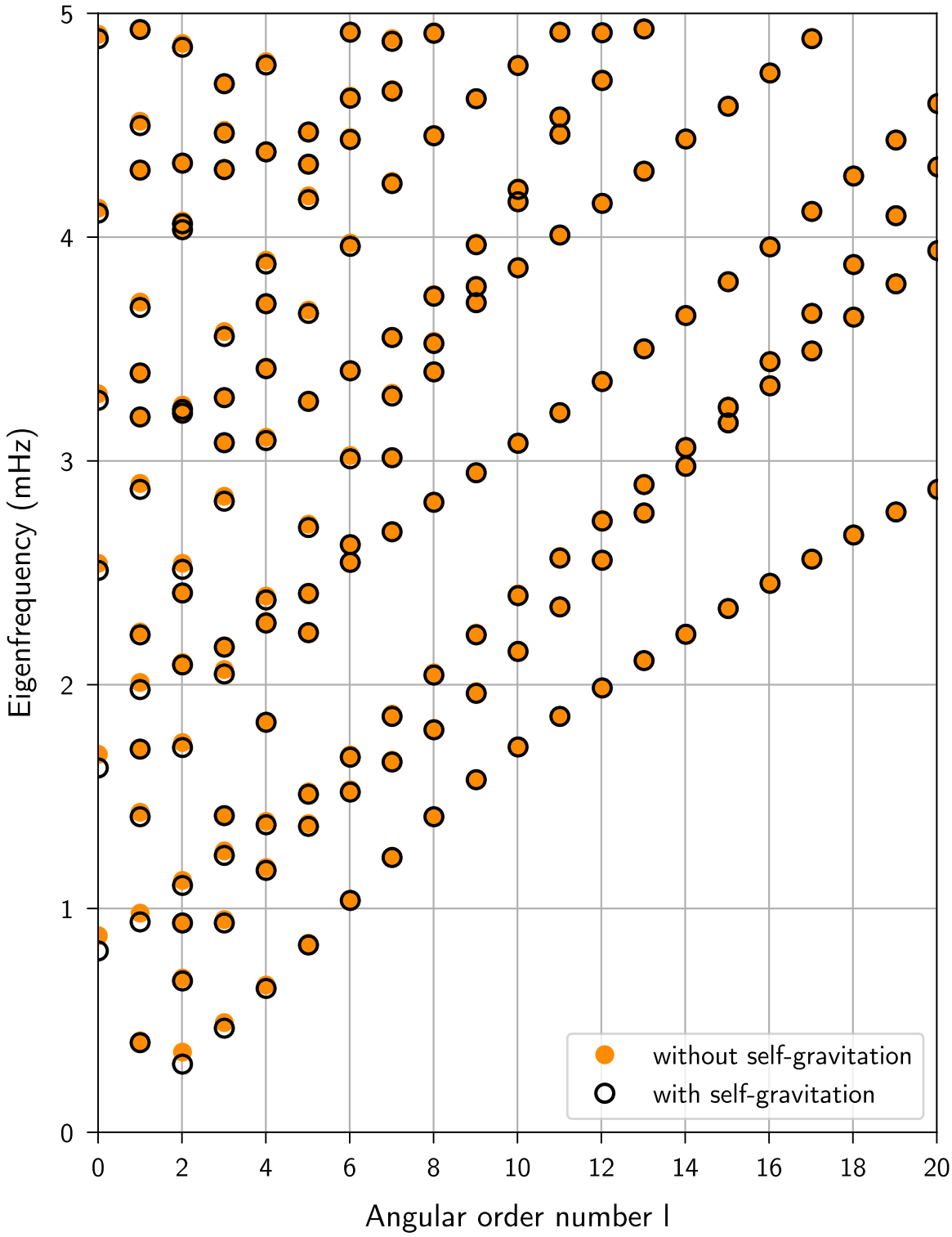

Figure A1. Dispersion diagram of spheroidal oscillations for an isotropic PREM model (no ocean), with (black dots) and without (orange dots) self-gravitation included. Self-gravitation effects are significant only at low frequencies and angular number ℓ.

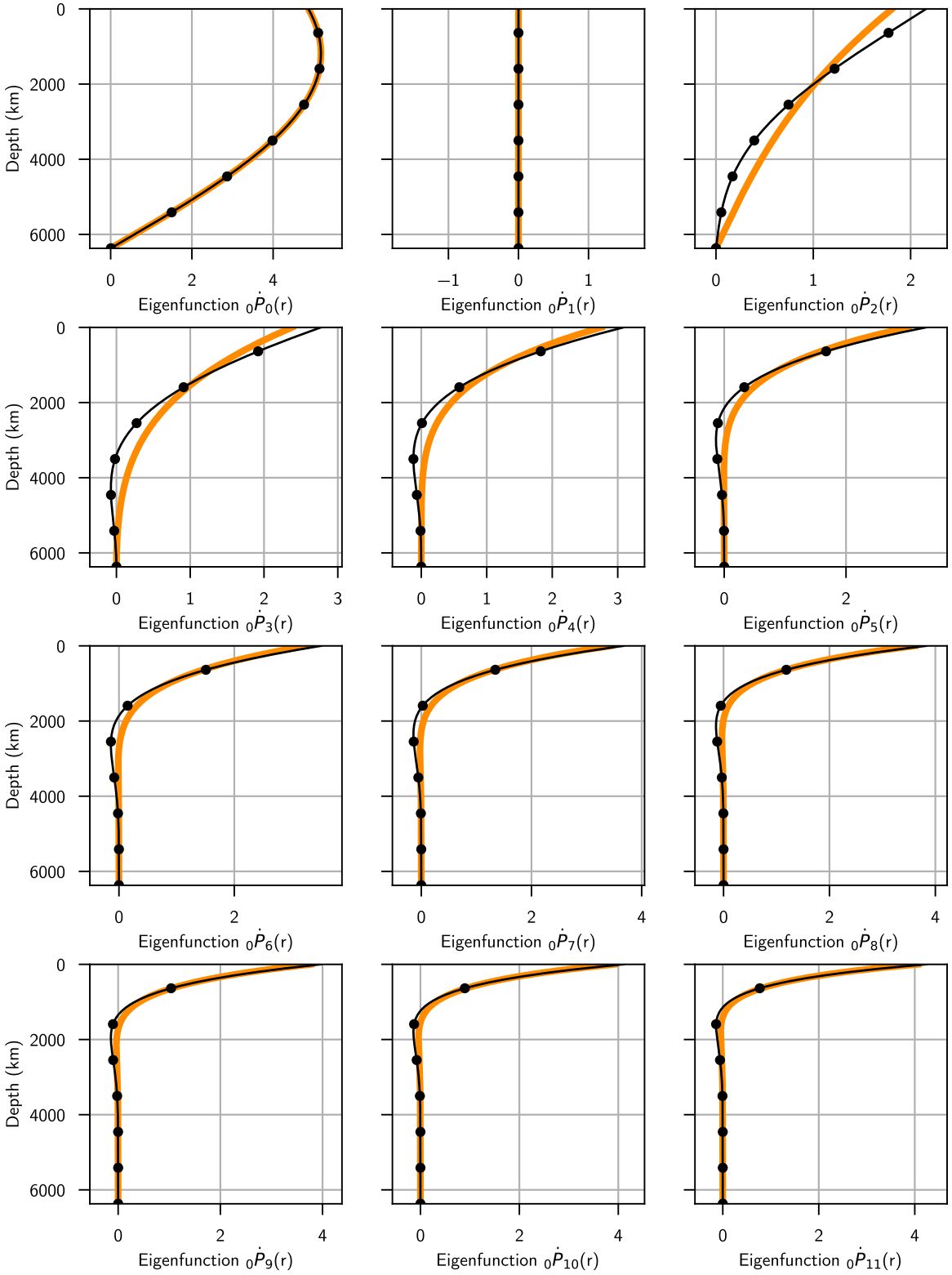

Figure A2. Eigenfunctions $\dot{\mathrm{P}}(r)$ within a homogeneous solid sphere, with (black lines) and without (orange lines) self-gravitation included. These are fundamental modes ($n = 0$) and the horizontal angular wavenumber ℓ ranges from 0 to 11. Self-gravitation effects are significant only at low frequencies. The $_0\mathcal{S}_1$ spheroidal mode is not computed, since it implies a displacement of the center of the Earth.

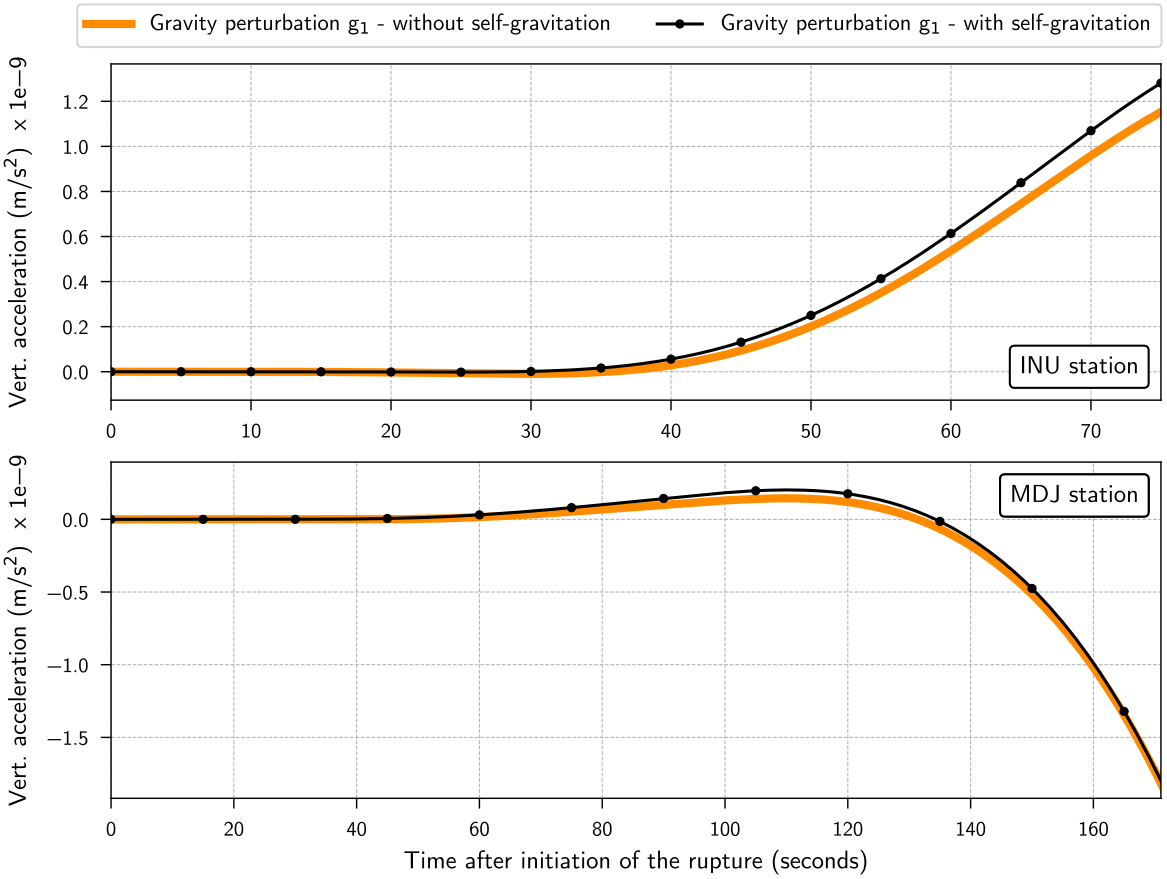

Figure A3. Vertical gravity perturbation induced by the M9.1 Tohoku earthquake, recorded at INU (top) and MDJ (bottom) stations, in a non self-gravitating (orange lines) and self-gravitating (black lines) isotropic PREM model (no ocean).

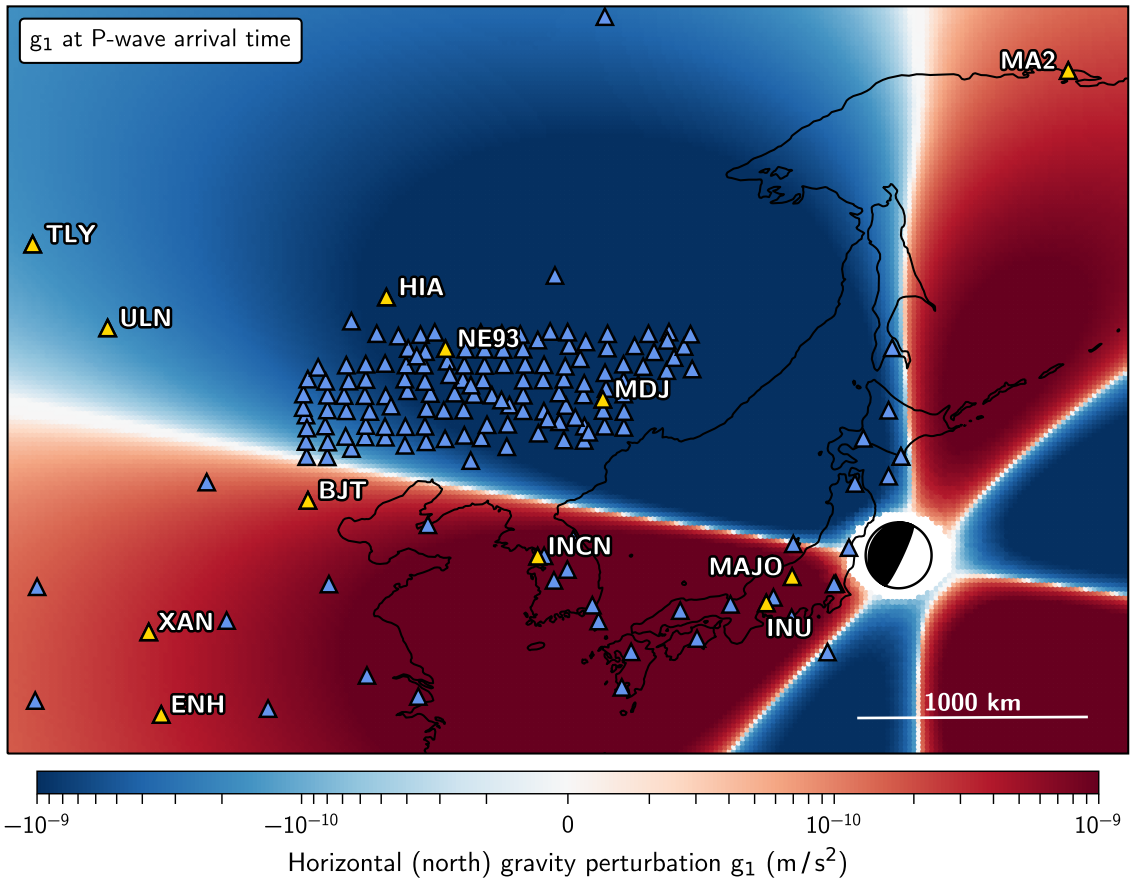

Figure A4. Horizontal (north) gravity perturbation g_1 induced at the Earth surface by the M9.1 Tohoku-oki earthquake, at P-wave arrival time. The focal mechanism locates the earthquake epicenter, and the triangles represent stations from the IRIS database. Yellow triangles are stations with low background seismic noise in the 30 minutes preceding the event. In the area close to the epicenter the simulations are less reliable due to the very short P travel times, and the perturbations are not computed.

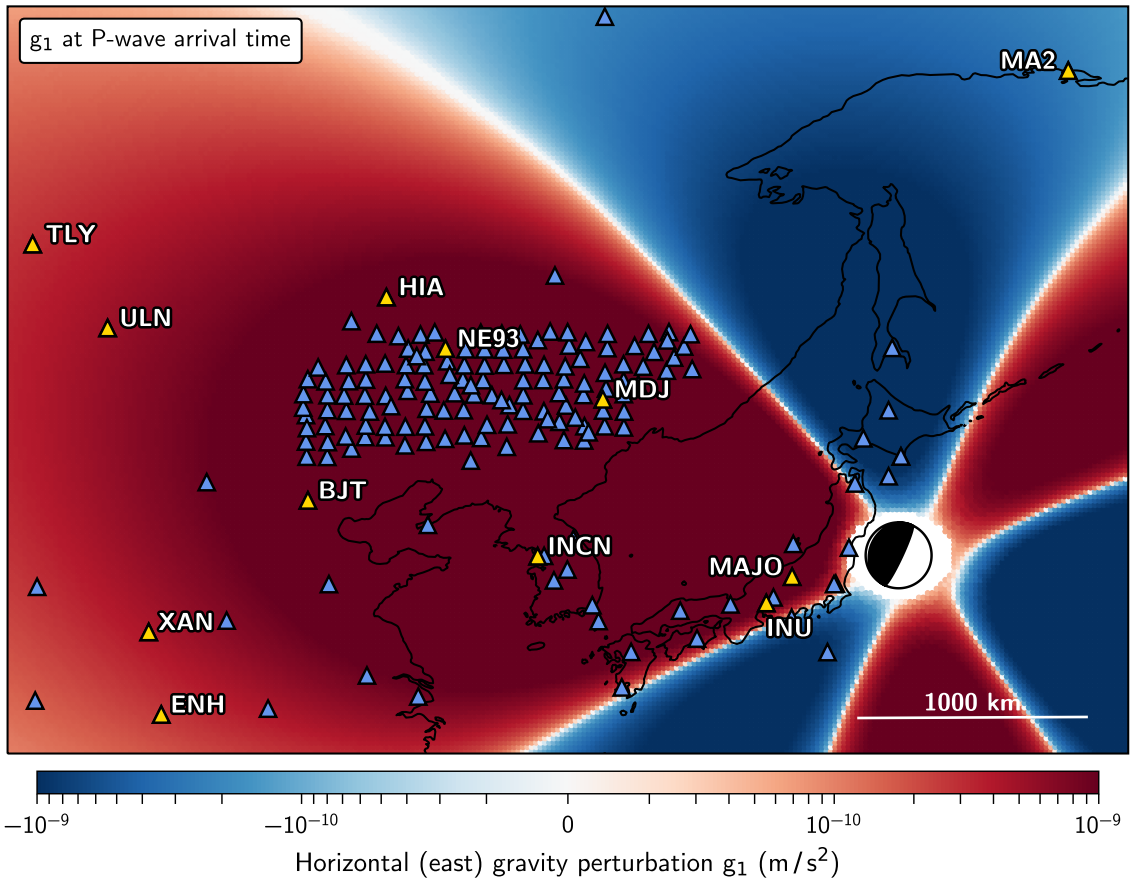

Figure A5. Horizontal (east) gravity perturbation g_1 induced at the Earth surface by the M9.1 Tohoku-oki earthquake, at P-wave arrival time. The focal mechanism locates the earthquake epicenter, and the triangles represent stations from the IRIS database. Yellow triangles are stations with low background seismic noise in the 30 minutes preceding the event. In the area close to the epicenter the simulations are less reliable due to the very short P travel times, and the perturbations are not computed.